2010 IEEE International Conference on Robotics and Automation
Anchorage Convention District
May 3-8, 2010, Anchorage, Alaska, USA

Hazard Analysis of Fracture-Reduction Robot and its Application to Safety Design of Fracture-Reduction Assisting Robotic System

Sanghyun Joung[1], Hongen Liao[1], Etsuko Kobayashi[1],
Mamoru Mitsuishi[1], Yoshikazu Nakajima[1], Nobuhiko Sugano[2], Masahiko Bessho[3],
Satoru Ohashi[3], Takuya Matsumoto[3], Isao Ohnishi[3], and Ichiro Sakuma[1]

Abstract— **In this paper, we discuss the issue of safety in robot-assisted fracture reduction. We define the hazards of robot-assisted fracture reduction and design safety control methods. Although a large reduction force is required to reduce femoral neck fractures, an unexpectedly large force produced by a robot may cause injury to the patient. We have designed two mechanical failsafe units and a software force limiter; this along with velocity control can guarantee a safe operation in reduction force. In addition, to reduce the movement of bone fragments as much as possible, we devised spatially constrained control methods for fracture-reduction robots. The fracture-reduction system was evaluated using simulated fracture reductions.**

I. INTRODUCTION

Hip fractures occur at the proximal end of the femur. The cause of most hip fractures is low-energy trauma, which is associated with falling from a standing height or lower, in elderly patients with osteoporosis. Using the epidemiologic literature on hip fracture incidence in various regions of the world and demographic projections, Cooper et al. estimated that the number of hip fractures occurring globally each year will rise from 1.66 million in 1990 to 6.26 million by 2050 [1].

Most patients with hip fractures undergo surgery. An operation comprises two processes: reduction and fixation of bone fragments. The fracture must be reduced before fixing the bone fragments, and pulling of bone fragment in this procedure requires a large reduction force. Conventional fracture reduction is often achieved using a fracture table. However, fracture tables have less degrees of freedom (DOF), which is one of the reasons why reduction is often inadequate. This may cause complications such as nonunion of the fracture [2]. Further, there are no safe methods available for avoiding the application of excessive force to the injured limb, which can lead to damage of the soft tissue around the bone fragment. Moreover, repeated exposure to radiation sustained by surgeons and medical staff is a well-known problem in the field of orthopedic surgery [3].

Füchtmeier et al. [4] introduced RepoRobo, a robotic system for assisting fracture reduction. They converted a commercial industrial robot for medical use by appropriate modifications. The requirements for using an industrial robot for reduction of femoral shaft fractures *in vitro* are well described. They did not, however, provide any experimental results. Westphal et al. [5] and references therein also tried to use an industrial robot for medical use. They tried to develop a surgical telemanipulator system to support long-bone fracture reduction procedures.

Studies prior to the work described in this paper were conducted by Mitsuishi et al. [6]. In Mitsuishi's system, the foot is fixed using a fracture boot, as in conventional fracture reduction methods. The authors have already reported navigation-based control of the system [7]. Another application of the proposed system is power assistance, where the robot augments the surgeon's force to generate the power required for fracture reduction. The reduction path and reduction force/torque also need to be controlled so that bone fracture reduction is conducted safely. In this study, we analyzed the hazards of robot-assisted fracture reduction in power assistance mode and designed countermeasures for hazard prevention. We then carried out an experimental evaluation of the proposed system for robot-assisted fracture reduction.

II. SAFETY AND SYSTEM DESIGN

In the case of an industrial robot, the major strategy for ensuring human safety is to physically separate the robot from vulnerable humans by creating a safe robot workspace from which humans are excluded. However, this strategy is obviously inappropriate in the case of a surgical robot, where the application demands interaction between the robot and humans in the same workspace and even direct operation on human subjects. Surgical robots must therefore have safety features that are appropriate to such applications in addition to the safety features currently required for industrial robot application.

A. Hazards of fracture reduction

Fig. 1 shows the hazards related to robot-assisted fracture reduction. The conventional method for fracture reduction is indirect reduction. A direct reduction method, which requires the insertion of external devices to fix the bone fragment, was devised to improve reduction accuracy, and a robotic system was introduced to assist surgeons in reducing fractures more accurately and steadily. Though the accuracy of the reduction can be increased by application of the new technique to the conventional method, the extended system also results

[1]Graduate School of Engineering, the University of Tokyo, 7-3-1 Bunkyo-ku, Tokyo, Japan, shjoung@bmpe.t.u-tokyo.ac.jp
[2]Graduate School of Medicine, Osaka University, Japan,
[3]Graduate School of Medicine, the University of Tokyo Hospital, Japan

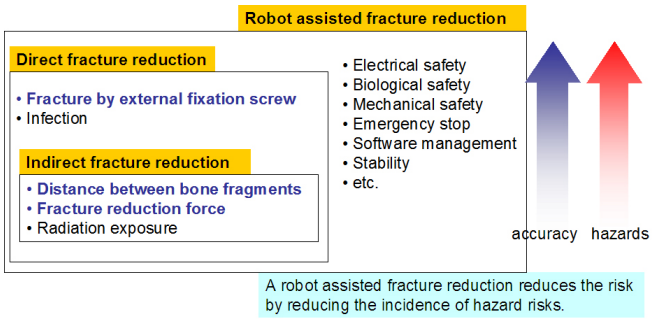

Fig. 1. List of hazards associated with robot-assisted fracture reduction

in an increase in the number of hazards. However, if the robotic system is able to control the hazards satisfactorily, the application of this system could increase reduction accuracy with lower risk. This paper presents an analysis of hazards in a robot-assisted fracture-reduction system for use in direct reduction methods, details of the implementation of safety countermeasures, and evaluation of results.

1) Distance between the bone fragments: Excessive traction may injure the sciatic nerve, which starts in the lower back and runs through the buttock and down the lower limb and serves nearly the whole of the skin of the leg, the muscles of the back of the thigh, and those of the leg and foot. Though traction motion of the limbs is required, it must be within a safe range. The safe range of traction distances recommended by surgeons is $25mm$ to $30mm$ between the proximal and distal bone fragments. A navigation system can measure the distance between the two bone fragments. A safe range can be kept by stopping the robot when the navigation system sounds an alarm for over-traction of the distal bone fragments. We have developed control software to provide constraints on robot motion to avoid excessive displacement of bone fragments.

2) Fracture-reduction force: Excessive reduction force may cause injury to the soft tissues of the limbs. Therefore, fracture-reduction robots need to have some functions that can limit the reduction force to a safe range. A fracture-reduction robot, named FRAC-robo, which is the predecessor of the fracture-reduction robot in this study, was used to monitor the traction force and the rotation torque in the reduction of proximal femoral fractures [9]. The average maximum traction force and rotation torque are $215.9N$ and $3.2Nm$, respectively. Although some clinical data have been reported, the safe range for fracture-reduction forces has not been clear up until now. A force limiter for controlling the fracture-reduction force has therefore been designed so that the force limit can be adjusted.

B. System design

We addressed the following two requirements when designing a robot to conduct fracture reduction with high levels of safety and accuracy:

- restriction of displacement of bone fragments to allowed values to prevent damage to soft tissues surrounding the bone and
- restriction of the applied force/torque on the bone fragment to avoid damage to the bone fragment.

In order to satisfy these requirements, we developed safety modules and a robot control method. The hardware layer of the robot has two mechanical failsafe units and a force sensor; the two mechanical failsafe units limit the reduction force, which is one of the system's hardware performance features. Data from force sensors are used to measure reduction force. The gain of the system speed controller was automatically adjusted to reduce the velocity of the fracture-reduction robot. Ensuring that there is little movement of the bone fragment can reduce the displacement of soft tissues around the bone fragment, thus, this reducing the risk of soft-tissue damage. A spatial constraint power assistance mode that constrains the rotation center at a point on the fracture surface of the bone fragment was developed to make highly accurate small movements of the bone fragment. The actual safety designs for these will be described in the next chapter.

III. Fracture-Reduction Assisting System

An example of the configuration of a fracture-reduction system is shown in Fig. 2. The fracture-reduction system consists of a fracture-reduction robot and a navigation system. The surgical bed and the fracture-reduction robot are arranged in a line. One side of the surgical bed is used for the navigation system, and the other side is used by the surgeon who reduces the fracture and fixes the bone fragments.

A. Fracture-reduction robot

The structure of the fracture-reduction robot is shown in Fig. 3(a); a kinematic model and the robot coordinates are provided in Fig. 3(b).

The fracture-reduction robot has six DOFs (i.e., three translation DOFs and three rotation DOFs). Three rotational axes intersect each other at one point, to give robot controls which are easily calculated kinematically. Translation along the y-axis and rotation around the y-axis has a mechanical failsafe unit which can mitigate excessive force. We installed a customized jig to fix the bone fragment to the robot. A

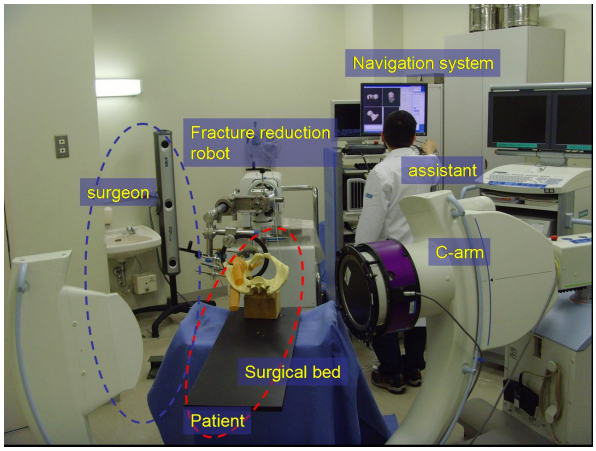

Fig. 2. Fracture-reduction system configuration

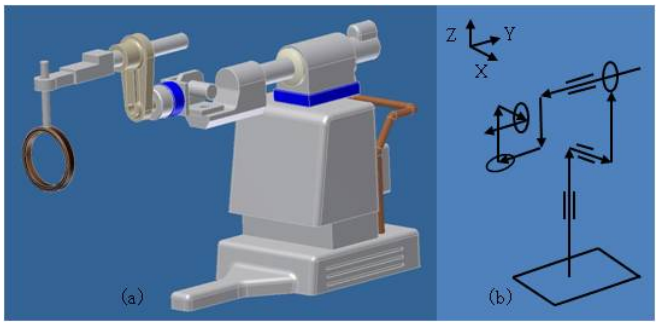

Fig. 3. Fracture-reduction robot; (a) outline, two blue parts show mechanical failsafe units and (b) kinematic model and coordinates of the robot

force-moment sensor (IFS-105M50A220-I63; Nitta, Osaka, Japan) is mounted on an end effector of the machine unit in order to monitor fracture-reduction forces and torques. The user interface is a touch panel. We installed four emergency buttons; all movements of the robot stop if a button is pressed. A four-color LED array bar shows the robot status: Power On, Ready, Operating, and Emergency Stop. Four steerable wheels attached beneath the robot enable medical staff to move the robot easily, in spite of its weight ($315kg$). The dimensions of the robot are 640 mm (width) $\times$ 1,084 mm (length) $\times$ 1,317 mm (height). This size makes it possible to transport the robot in a normal passenger elevator.

B. Mechanical failsafe unit

Excessive reduction force may injure soft tissues of the limbs. The fracture-reduction robot must therefore have mechanical units that can limit the reduction force to a safe range. The robot has two mechanical failsafe units, which can mitigate excessive reduction forces. The installed positions of them are illustrated with blue parts in Fig. 3(a). These units maintain high rigidity within the allowed force and torque ranges. However, if an excessive force is applied to the unit, it decouples the end effector of robot from the actuation unit to remove the applied force or torque and prevent excessive force, which might damage the soft tissues, on the bone fragment. The longitudinal direction of the bone fragment coincides approximately with the traction direction of the robot. Surgeons should ensure that these positional relations are correct as the first step in surgery. If these positional relations are ensured, the traction failsafe unit can limit the traction force of the bone fragment, and the rotation failsafe unit is in operation while internal or external rotation of the bone fragment is conducted. Though Warisawa et al. [8] had reported the mechanical failsafe for an indirect fracture redution, we modified the units for a direct fracture reduction and described more details about these units.

The traction failsafe unit is installed on the y-axis of the fracture-reduction robot; this unit has a plunger with a steel roller pushed into a hollow by a spring (Fig. 4). The threshold force can be adjusted from $200N$ to $400N$ by adjustment of the screw, which can change the spring compression force.

The rotational failsafe unit is mounted between the customized jig and the tip of the robot. The mechanism is

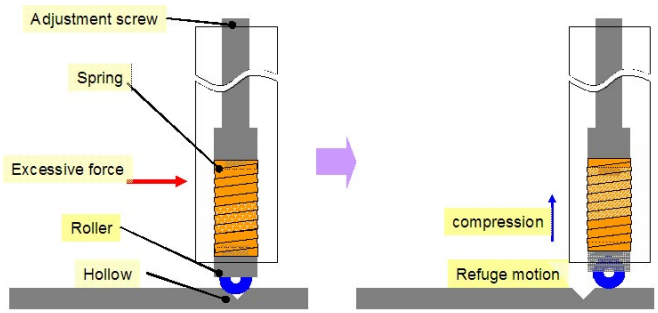

Fig. 4. Structure of translational failsafe mechanism

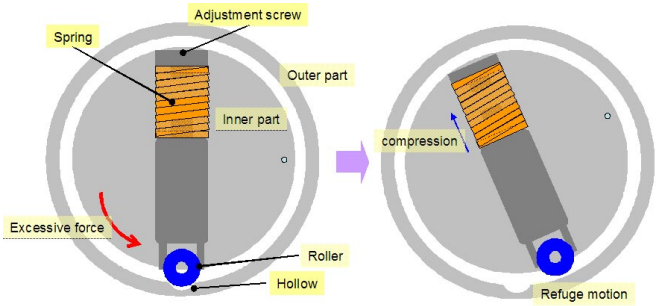

Fig. 5. Structure of rotational failsafe mechanism

similar to that of the traction failsafe unit, as shown in Fig. 5. The threshold is adjustable from $20Nm$ to $40Nm$ by controlling the length of the spring. When the unit is decoupled, the rotation range of the customized jig is constrained by mechanical stoppers, the positions of which can be varied from 30° to 120°.

A threshold can be calculated by considering the equilibrium of force and moment with two parameters, the spring force and the contact angle between a roller and a hollow. Fig. 6 shows the forces acting on the roller. F_s is the spring force. F_{ex} is the external force. N is the vertical component of force acting on a contact point between the roller and the hollow and is equal to F_s. W denotes the horizontal component of force acting on the contact point and is equal to F_{ex}. The following equation can be found by considering the moment equilibrium at the center of the roller

$$F_s r \sin\theta = F_{ex} r \cos\theta \tag{1}$$

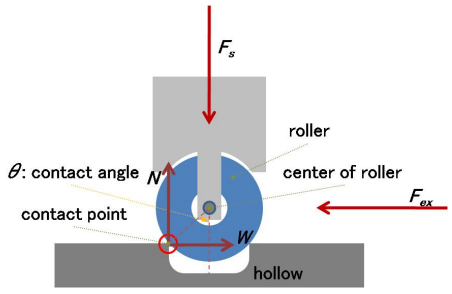

Fig. 6. Forces acting on roller and hollow

Here r is the radius of the roller and θ is the contact angle. From (1), the spring force for constraining the given F_{ex} can obtained by

$$F_s = kx = \frac{F_{ex}}{\tan\theta} \tag{2}$$

Here, k denotes the spring constant and x is the displacement of spring. A similar idea can be applied to the rotational failsafe unit, which gives

$$F_s = \frac{F_{ex}}{R\tan\theta} \tag{3}$$

Where, R is the radius of the inner part of rotational failsafe unit. Specifications for the mechanical failsafe units are shown in Table I. From (2) and Table 1, $2.5mm$ displacement of the spring made by the adjust screw is needed to set the threshold to $200N$ and $4.9mm$ displacement is required for $400N$ with the translational failsafe unit. We selected an adjust screw with the pitch of $3.0mm$. It is larger than the difference between above two displacements, so that we can adjust thresholds within single rotation of the adjustment screw. A similar idea was applied to the rotational failsafe unit.

TABLE I
SPECIFICATION FOR THE MECHANICAL FAILSAFE UNITS

		translation	rotation
Threshold range, N or Nm		200-400	20-40
radius of roller, mm		9.5	8
contact angle, °		34	45
spring	constant, N/m	121	204
	allowable displacement, mm	14.7	6.8
adjustment screw (pitch, mm)		M27 (3.0)	M22 (2.5)
radius of inner part, mm			50

The performances of the two failsafe units were evaluated. The end effector of robot was pulled out or was rotated by a human until the failsafe unit was activated, and the maximum force was recorded using the force sensor. Traction direction thresholds were set at $\pm200N$, $\pm300N$, and $\pm400N$ at each evaluation. The rotational direction thresholds were set at $\pm200Ncm$, $\pm300Ncm$, and $\pm400Ncm$. Five tests were conducted at each threshold. Fig. 7 shows the evaluation results. The variation in each of the five trials is shown by a bar. In the case of the traction direction, it was found that the test values were significantly smaller than the set values; the set value is the value at which the threshold is set, and the test value is the experimental result for the set value. This difference results from the weakened offset tension of the spring, which occurs when the robot is reassembled for correction of movement. The difference may be reduced by adjusting the offset tension. Long-term performance should be evaluated considering the variation of the offset tension and the durability of the mechanical structure.

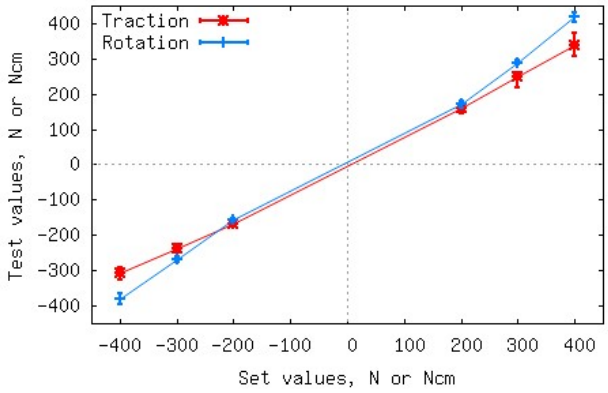

Fig. 7. Performance of failsafe mechanism, n=5

C. Software force limiter

The software force limiter is also designed to prevent excessive reduction force. The velocity gain is controlled against the measured force, as shown in (4).

$$G(t) = \begin{cases} 1 & F(t) < Th1 \\ \frac{(F(t)-Th1)^2}{(Th2-Th1)^2} & Th1 \leqq F(t) < Th2 \\ 0 & F(t) \geqq Th2 \end{cases} \tag{4}$$

Here, $F(t)$ is the measured fracture-reduction force, $Th1$ and $Th2$ are the first and second thresholds of the software limiter, and $G(t)$ is the velocity gain. Two thresholds are used, not only to avoid sudden stopping of the robot, but also to forewarn the operator of an increase in the reduction force by decelerating the robot. The robot speed is calculated using (5) and is slowed down according to a quadratic curve between the two thresholds.

$$V(t) = \alpha G(t) F(t) \tag{5}$$

Here α is a weighting factor and $V(t)$ is the control velocity of the robot. We set two thresholds of the software force limiter below the limiting force of the mechanical failsafe mechanism so that excessive force can be mitigated by the software force limiter. However, the mechanical failsafe mechanism is only operated when software problems occur.

The software force limiter was evaluated using a static obstacle. The robot moved in the direction of the x-axis, and the robot's velocity was set at $10mm/s$. A static obstacle was placed beside the customized jig to increase the reaction force. Two thresholds were set at $100N$ and $150N$, respectively. The robot's position was recorded with the robot's rotary encoder, and the reaction forces were measured using a built-in force sensor with a frequency of $50Hz$.

Fig. 8 shows the variations in the measured force and in the velocity. The jig contacted the obstacle within $5s$, and the force increased slowly. The force approached the first threshold at about $7s$, and the speed of the robot slowed down with the designed gain. The robot was stopped as

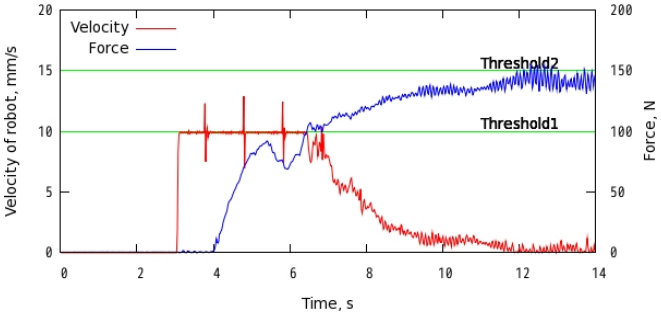

Fig. 8. Evaluation results for the software force limiter

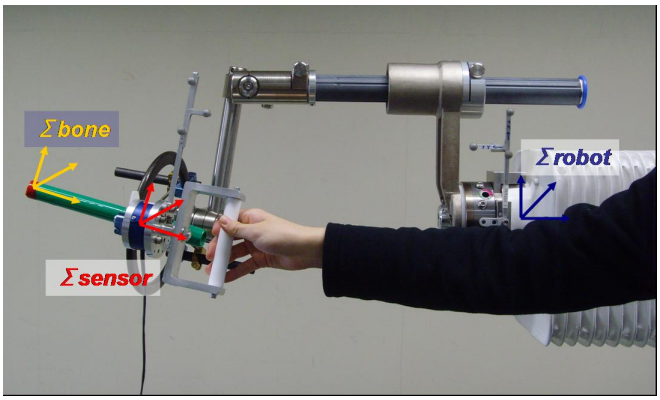

Fig. 9. Configuration of direct fracture reduction using fracture-reduction robot

the force reached the second threshold. Some spikes can be found in the velocity variation. The rotary encoder signals were recorded as a user-level task (non-real-time process) so as not to interrupt the main process. Thus the measurement frequency of $50Hz$ was not guaranteed. This is considered to be one cause of the spikes. This should be reconfirmed using a real-time measurement system. The usefulness of the software force limiter will be evaluated from a simulated fracture reduction with manual operation of the robot.

D. Control method for safe power assistance by the robot

In common hip fracture cases, the distal bone fragment is pulled up to the upper body and rotated externally by the influence of soft tissues. The surgeon therefore draws the distal bone fragment and then rotates it internally to reduce the fracture. The fracture-reduction robot reduces the fracture by a similar process, and provides an intuitive control method: a spatially constrained power assistance mode. Compared with indirect reduction methods, direct methods provide a larger number of DOFs for manipulating the bone fragments. However, direct methods also generate additional risks of damage to soft tissues and bone fragments (in particular at the bone/insertion pin interface).

To achieve safe direct fracture reduction, constraints on the bone fragment trajectory should be properly applied by surgeons to bone fragment manipulation.

We therefore introduced the following control method. In the proposed control method, the fracture-reduction robot can move each axis of the robot center on the bone coordinates. The origin of the bone coordinates is at the center of the fracture surface, and its primary axis is aligned with the longitudinal direction of the bone fragment. Surgeons can track the bone fragment along its longitudinal direction or can rotate the bone fragment centering on one point; these movements are safer and more intuitive than movement centered on the robot's coordinates. We abbreviated this control mode 'RCC-PA'(Rotation Center Constrained Power Assistant). The algorithm is as follows. The method supposes that the force and moment applied to the bone fragment by the surgeon are in his intended direction of movement, and that the magnitude of the force or moment is proportional to the velocity of the bone movement. The play of each axis is then calculated by considering the bone fragment and the robot as a rigid body. The problems to be solved are how to measure the force given to the bone fragment and how to measure and decide the bone's coordinates.

An additional force sensor (IFS-67M25A50-I40; Nitta, Osaka, Japan) was installed to measure the force given to the bone fragment, as shown in Fig. 9. The sensor was positioned between the handle and the ring-type frame holding the external fixation screws. The surgeon controls the bone fragment using the handle. The navigation system will be used to determine the bone's coordinates [10]. The navigation system measures and integrates the coordinates of the robot, the force sensor, and the fluoroscope, and calculates the coordinates using 2D-3D registration. The fracture-reduction robot receives the coordinate information from the navigation system. The force given to the bone fragment can be calculated using (6).

$$\begin{bmatrix} {}^{B}\mathbf{f} \\ {}^{B}\mathbf{m} \end{bmatrix} = \begin{bmatrix} {}^{B}\mathbf{R}_S & \mathbf{0} \\ [{}^{B}\mathbf{P}_S\otimes]\,{}^{B}\mathbf{R}_S & {}^{B}\mathbf{R}_S \end{bmatrix} \begin{bmatrix} {}^{S}\mathbf{f} \\ {}^{S}\mathbf{m} \end{bmatrix} \tag{6}$$

Here,

$$if\ \mathbf{a} = \begin{bmatrix} a_x \\ a_y \\ a_z \end{bmatrix},\ [\mathbf{a}\otimes] = \begin{bmatrix} 0 & -a_z & a_y \\ a_z & 0 & -a_x \\ -a_y & a_x & 0 \end{bmatrix} \tag{7}$$

${}^{\mathbf{A}}\mathbf{f}$(or ${}^{\mathbf{A}}\mathbf{m}$) is the force(or moment) at the given coordinates of "A". And ${}^{\mathbf{A}}\mathbf{R}_{\mathbf{B}}$ and ${}^{\mathbf{A}}\mathbf{P}_{\mathbf{B}}$ are the rotation matrix and the translation matrix, respectively. "S" denotes sensor coordinates and "B" denotes bone coordinates. And we used subscripts of "o", "p", and "g" to abbreviate the expressions of "original position", "present position", and "goal position", respectively.

Then, ${}^{B_p}\mathbf{T}_{B_g}$, a translation matrix from the present bone coordinate to the surgeon's target bone coordinate, is calculated from ${}^{\mathbf{B}}\mathbf{f}$ and ${}^{\mathbf{B}}\mathbf{m}$ using (8).

$$
\begin{aligned}
{}^{B_p}\mathbf{T}_{B_g} &= \begin{bmatrix} {}^{B_p}\mathbf{R}_{B_g} & {}^{B_p}\mathbf{P}_{B_g} \\ \mathbf{0} & 1 \end{bmatrix} \\
{}^{B_p}\mathbf{R}_{B_g} &= \begin{bmatrix} k_x k_x vt + ct & k_x k_y vt - k_x st & k_x k_z vt + k_y st \\ k_x k_y vt + k_x st & k_y k_y vt + ct & k_y k_z vt - k_x st \\ k_x k_z vt - k_y st & k_y k_z vt + k_x st & k_z k_z vt + ct \end{bmatrix} \\
{}^{B_p}\mathbf{P}_{B_g} &= {}^{B}\mathbf{f}
\end{aligned} \tag{8}
$$

Here st, ct and vt denote $\sin(t)$, $\cos(t)$ and $1-\cos(t)$, respectively. $\mathbf{R}$ is the rotation of t° around the rotation axis, $\mathbf{K}$, which is given by (9). The t is proportional to $|{}^{B}\mathbf{m}|$.

$$
\mathbf{K} = \begin{bmatrix} k_x \\ k_y \\ k_z \end{bmatrix} = \frac{1}{|{}^{B}\mathbf{m}|}{}^{B}\mathbf{m} \tag{9}
$$

${}^{B_p}\mathbf{R}_{B_g}$ or ${}^{B_p}\mathbf{P}_{B_g}$ is set as $\mathbf{I}$ or $\mathbf{0}$ in order to separate translational movement and rotational movement during fracture reduction.

The ${}^{R_p}\mathbf{T}_{R_g}$, which describes translation from the present robot position to the goal position, can be calculated from the given coordinates and ${}^{B_p}\mathbf{T}_{B_g}$ using (10).

$$
{}^{R_o}\mathbf{T}_{R_g} = {}^{R_o}\mathbf{T}_{R_p}\,{}^{R_p}\mathbf{T}_{B_p}\,{}^{B_p}\mathbf{T}_{B_g}\,{}^{B_g}\mathbf{T}_{R_g} \tag{10}
$$

${}^{B_g}\mathbf{T}_{R_g}$ is the inverse matrix of the ${}^{R_p}\mathbf{T}_{B_p}$, because the positional correlation between the bone and the robot is not changed when the robot is moved.

${}^{R_o}\mathbf{T}_{R_g}$ can be expressed as six parameters, i.e., three translations and three rotations, and the present position of the robot is calculated by reading the six rotary encoders of the axis. Then, the difference between the present position and the goal position gives the distance moved for each axis.

The accuracy of the RCC-PA method was evaluated. The bone, sensor, and robot coordinates were set using an optical 3D position measurement system (Polaris; NDI, Waterloo, Ontario, Canada). The origin position of the bone coordinate was measured in the robot coordinate as the RCC-PA was being conducted. The ideal movement is zero. We therefore treat the distance moved by the origin of the bone coordinate from the initial position as the control error. The movement of the axis influences the control error because the fracture-reduction robot is a serial construct. Each movement of the axis is also measured to estimate these effects.

Fig. 10 shows the control error and the play of each axis. The control error is within $2mm$ and is less than the play of the axis. Both quantities are larger at the x- and z-axes, which are related to the rotation axis.

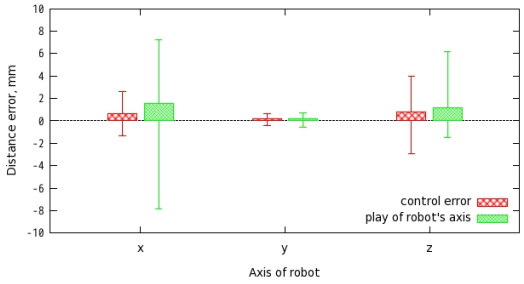

Fig. 10. RCC-PA motion distance error

IV. Experiments

The developed fracture-reduction system was evaluated by simulated fracture reduction using hip fracture models. The hip fracture model was prepared by cutting a femur model (Composite Femur; Pacific Research Laboratories, Inc., Vashon, WA, USA) with a band saw, and attaching a rubber band between the femur and the hip to simulate the influence of muscles such as the gluteus medius and the piriformis.

A fracture reduction is generally assessed using 2D fluoroscopic images. The reduction alignment angles of the anteroposterior (AP) and lateral views should be within the defined values; however, this assessment is influenced by the measured angle of the fluoroscopic images, as well as by the surgeon's viewpoint. Therefore, to ensure high reproducibility, we evaluated the reduction results from parameters related to the mechanical axis used to assess the femur deformity [11]. The mechanical axis is drawn from the center of the knee joint to the head of the femur. If the mechanical axis is defined, the mechanical distal femur angle (DFA) and the proximal femur angle (PFA) can also be defined. DFA is the angle between the mechanical axis and a tangent through the two most convex distal points of the femoral condyles, and PFA is the angle between the mechanical axis and a line from the tip of the greater trochanter to the hip center. Before fracturing the femur model, we marked feature points such as the greater trochanter, the head of the femur, the lateral condyle, and the medical condyle. We measured the 3D positions of the feature points using a pen-type reference marker and the optical 3D position measurement system. We then calculated the normal values of the length of the mechanical axis, the PFA, and the DFA from the four measured feature points. The reduction values after the fracture reduction were compared to the normal values.

A. Experimental setup

The fracture model was positioned on the surgical bed. The customized jig for connecting the bone fragment to the robot was positioned near the fracture model using a jog operation and the distal bone fragment of the fracture model was connected to the jig.

Fracture reduction using the RCC-PA mode was conducted eight times in open conditions, which means that the fracture site could be seen directly. The fracture-reduction procedure was divided into three steps as follows. First, longitudinal traction of the distal bone fragment was performed. Second, the posture of the distal bone fragment was modified. The main movement was internal rotation of the bone fragment while the center of rotation was constrained. Finally, the distal bone fragment was repositioned, and fine control of the alignment was carried out.

The time required for fracture reduction was measured. The robot movements and the reduction forces/moments

were recorded at each trial. The distal bone fragment was also traced using the optical 3D position measurement system.

Two thresholds of software force limiter were set with respect to the developed force of the fracture model. The first threshold was set at $60N$ and the second threshold was set at $100N$ so that the robot could move freely with the reduction force of $60N$, the speed of the robot slowed down inversely with an increase in the reduction force, and the robot was stopped when the reduction force reached $100N$. The fracture reductions of the fracture model were reduced using the proposed methods, either with or without the software force limiter, and the movement of the bone fragment and the reduction force were compared.

B. Results

Fig. 11 shows the variations in the traction distance of the bone fragment and the reduction force during the simulated fracture reduction with and without the software force limiter. The horizontal axis is time (ms). The fracture reduction was conducted in three stages. In the first stage, the translational displacement was increased as the distal bone fragment was pulled out. As a result, the resulting force and the resulting moment were also increased. Rotation of the bone fragment was conducted during the second stage. The position and posture of the distal bone fragment was fine tuned during the third stage.

The reduction forces were always below the second threshold ($100N$) using the software force limiter, while the reduction forces were above this value without the software force limiter.

Fig. 12 shows the "before" and "after" status of the fracture model. The average time for the fracture reduction was $82.5s$, and the difference from the normal value of the mechanical axis is shown in Table II.

V. Discussion and Conclusion

Simulated fracture reduction was conducted using the RCC-PA mode of the fracture-reduction robot. A software force limiter using two threshold levels can prevent excessive force during simulated fracture reduction. Two threshold levels were set for the resultant force produced by the fracture model. The reduction force was $100N$ when the distal bone fragment was under traction up to $30mm$, which is in the range that is safe from over-traction. Thus, the second threshold was set at $100N$ to avoid over-traction of the distal bone fragment. The first threshold was set at $60N$, and provides information on proximity to the second threshold by a reduction in robot speed. The RCC-PA mode with the software force limiter function can reduce the fracture model without affecting the reduction motion of the robot while the reduction forces are within the second threshold. Feeling timing of the speed reduction was not evaluated. Further, this varies among different individuals. The first threshold and the speed gain slope should be modified from these data.

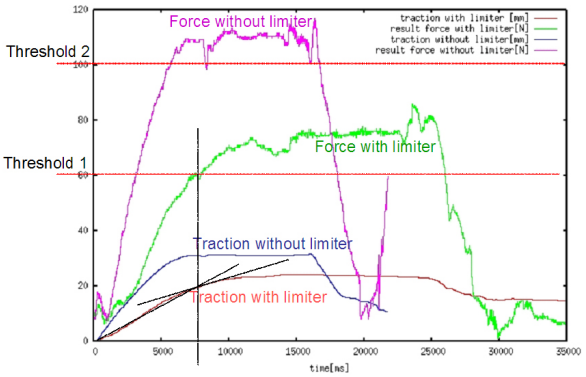

Fig. 11. Variations in traction distance and reduction force during simulated fracture reduction

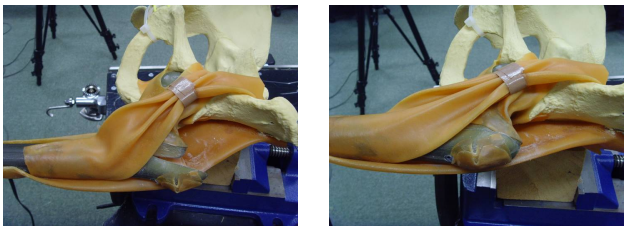

(a) (b)

Fig. 12. Results of fracture reduction using the RCC-PA method: (a) before reduction and (b) after reduction.

TABLE II

Fracture-reduction results with RCC-PA. ( ) is the difference between the noraml value and the reduction value

Parameter	Normal	Reduction value		
		ave	min	max
PFA, °	88.14	87.81(0.79)	86.84(0.32)	89.28(1.30)
DFA, °	90.60	90.89(0.34)	90.45(0.04)	91.34(0.74)
MA, mm	426.78	427.76(1.06)	426.44(0.26)	428.88(2.10)

Threshold values must be validated using clinical data. Maeda et al. reported some reduction force clinical data [9]. However, the data were obtained from healthy subjects, using an indirect reduction method. Although these data should be considered to determine the threshold, they cannot be used to determine the threshold. Additional clinical data are required; this is an ongoing project.

A fracture-reduction procedure is generally considered accurate and precise when the alignment error and the gap are within $2°$ and $2mm$, respectively, according to assessments based on 2D imagery. The average differences in PFA, DFA, and MA after fracture reduction using the RCC-PA mode were $0.79°$, $0.34°$, and $1.06mm$, respectively (n=8). Although there are no recommended values for the evaluation methods used in this paper, it is believed that differences are allowable when comparing the 2D recommended values, and that the RCC-PA mode has the potential to reduce fractures with high precision.

The robot can be controlled intuitively, which means that the operators can move the bone fragment easily in the

intended manner. A surgeon who used the RCC-PA mode commented as follows:

- It was good that the fracture could be reduced using a small force.
- By constraining the rotation center, the fracture could be reduced easily and intuitively.
- The method should be evaluated using the fracture model with a rough fracture surface.

All trials were conducted under open conditions. In a clinical situation, the operator has to depend on the navigation system or fluoroscope to confirm the status of the fracture site. Therefore, the RCC-PA mode should also be evaluated in a blind situation.

We have presented safety controls for systems for assisting fracture reduction. A simulated fracture reduction was conducted using the RCC-PA mode with a software force limiter. The fracture model used in the evaluation produces reaction forces, and the accuracy of the RCC motion under the effect of the load was also evaluated. A software force limiter with two threshold levels could successfully mitigate excessive reduction. Although the results show the potential to reduce fractures with high precision, additional safety features should be developed and evaluated for clinical use of the developed system.

VI. ACKNOWLEDGMENTS

The authors thank THK CO., LTD. (JAPAN) for providing technical support to the fracture-reduction robot; Mr. Hongho Kim (Dept. Precision Engineering, the University of Tokyo) for his skilled illustration. This work was supported by Health Labour Sciences Research Grant.

REFERENCES

[1] Cooper, C., Campion, G., and Melton, L. J., "Hip fractures in the elderly: A world-wide projection", *Osteoporosis International*, vol. 2, 1992, pp. 285-289.

[2] M. J. PARKER and C.E. TAGG, "Internal fixation of intracapsular fractures", *Journal of the Royal College of Surgeons of Edinburgh*, vol. 47, 2002, pp. 514-547.

[3] L.P.Müller, J.Suffner, K.Wenda, W.Mohr, and P.M.Rommens, "Radiation exposure to the hands and the thyroid of the surgeon during intramedullary nailing", *Injury*, vol. 29, 1998, pp. 461-468.

[4] Bernd Füchtmeier, Stefan Egersdoerfer, Ronny Mai, Rainer Hente, Daniel Dragoi, Gareth Monkman, and Michael Nerlich, "Reduction of femoral shaft fractures in vitro by a new developed reduction robot system 'RepoRobo'", *Injury*, vol. 35, 2004, pp. 113-119.

[5] Ralf Westphal, Simon Winkelbach, Friedrich Wahl, Thomas Gösling, Markus Oszwald, Tobias Hüfner, and Christian Krettek, "Robot Assisted Long Bone Fracture Reduction", *Int J of Robotics Research*, Vol. 28, 2009, pp.1259-1278.

[6] M.Mitsuishi, N.Sugita, S.Warisawa, T.Ishizuka, T.Nakazawa, N.Sugano, K.Yenenobu, and I.Sakuma, "Development of a computer-integrated femoral head fracture reduction system", *In Proceedings of ICM '05.*, 2005, pp. 834-839.

[7] Sanghyun Joung,Hirokazu Kamon, Hongen Liao, Junichiro Iwaki, Touji Nakazawa, Mamoru Mitsuishi, Yoshikazu Nakajima, Tsuyoshi Koyama, Nobuhiko Sugano, Yuki Maeda, Masahiko Bessho, Satoru Ohashi, Takuya Matsumoto, Isao Ohnishi, and Ichiro Sakuma, "A Robot Assisted Hip Fracture Reduction with a Navigation System", *In Proceedings of MICCAI 2008*, 2008, pp. 501-508.

[8] S. Warisawa, T. Ishizuka, M. Mitsuishi, N. Sugano, K.Yonenobu, and T.Nakazawa, "Development of a femur fracture reduction robot", *In Proceedings of ICRA 2004*, vol. 4, 2004, pp. 3999-4004.

[9] Y.Maeda, N.Sugano, M.Saito, K.Yonenobu, I.Sakuma, Y.Nakajima, S.Warisawa, and M.Mitsuishi, "Robot-assisted femoral fracture reduction: Preliminary study in patients and healthy volunteers", *Computer Aided Surgery*, vol. 13, 2008, pp. 148-156.

[10] Y.Nakajima, T.Tashiro, N.Sugano, K.Yonenobu, T.Koyama, Y.Maeda, Y.Tamura, M.Saito, S.Tamura, M.Mitsuishi, N.Sugita, I.Sakuma, T.Ochi, and Y.Matsumoto, "Fluoroscopic bone fragment tracking for surgical navigation in femur fracture reduction by incorporating optical tracking of hip joint rotation center", *IEEE Transactions on Biomedical Engineering*, vol. 54, 2007, pp. 1703-1706.

[11] Paley D., *Principles of deformity correction*, Berlin: Springer, 2001.